Journal of Marine Systems 227 (2022) 103697

Contents lists available at ScienceDirect

Journal of Marine Systems

journal homepage: www.elsevier.com/locate/jmarsys

Large scale patches of *Calanus finmarchicus* and associated hydrographic conditions off the Lofoten archipelago

Nicolas Weidberg [a,*,1], Nestor Santana Hernandez [a], Angelika H.H. Renner [b], Stig Falk-Petersen [c], Sünnje L. Basedow [a]

[a] Department of Arctic and Marine Biology, UiT The Arctic University of Norway, N-9019 Tromsø, Norway
[b] Institute of Marine Research, Fram Centre, N-9296 Tromsø, Norway
[c] Akvaplan-niva, Fram Centre, N-9296 Tromsø, Norway

ARTICLE INFO

Keywords:
Zooplankton aggregations
Copepods
Spatial autocorrelation
Diel vertical migration
Sea level anomaly

ABSTRACT

Large swarms of individuals at different spatiotemporal scales characterise the distributions of many animal species. In the ocean several mesozooplankton taxa aggregate in large patches or swarms driven by active behavioural responses to hydrographic structures, although intrinsic biotic characteristics of species' life cycles not related with the environment can also affect spatial distributions. To understand the mechanisms of aggregation and disentangle environmental and pure spatial effects contributing to patch formation, we extensively sampled a large *Calanus finmarchicus* patch off the Lofoten islands, northern Norway, in spring 2017 by means of Laser Optical Plankton Counter (LOPC) cross shelf transects and biophysical samplings at fixed stations. We observed a clear association between the buoyant layer of the fresh, cold Norwegian Coastal Current (NCC) and high surface copepod abundances. Off shelf lateral displacements of the NCC along its path may retain copepods from the offshore basins. At deeper layers, copepod abundances increased markedly at regions with low sea level anomalies and reduced vertical flows. Our results also suggest that copepods performed short range diel vertical migration within the patch. Potential future changes in the seasonality and structure of the NCC and their impact on swarm occurrence and formation are discussed.

1. Introduction

Aggregations of large numbers of individuals in clearly defined regions are characteristic of many animal taxa from insects to ungulates in response to different biotic and abiotic factors (Krause and Ruxton, 2002; Morrell and James, 2008). In the pelagic realm, zooplankton swarms, defined as aggregations much denser than background concentrations (Ueda et al., 1983), have been known since the 19th century. These large and persistent features started to be studied because of their importance for fisheries and general ecosystem functioning (Hardy and Gunther, 1935; Hamner et al., 1983; Folt et al., 1999). In addition, marine ecologists got concerned about the effect of patchiness on the estimation of plankton abundances (Fasham, 1978), and efforts to understand the ultimate causes of zooplankton swarm formation increased.

In parallel with the inclusion of patchiness in ecological studies on zooplankton, sonar and acoustic readings across the oceans and fjords revealed clear and widespread zooplankton diel vertical migration (Falk-Petersen and Hopkins, 1981; Folt et al., 1999; Fornshell and Tesei, 2013). The active swimming behaviour required for such migrations showed that zooplankton could overcome weak vertical currents in the order of a few mm s^{-1}, especially at convergent fronts where they accumulate in high abundances (Pineda, 1999; Shanks et al., 2005; Genin et al., 2005; Shanks and Shearman, 2009; Weidberg et al., 2014). Thus, it is the interaction between zooplankton behaviour and aggregating physical structures at different spatiotemporal scales which eventually leads to swarms (Haury et al., 1978; Mackas et al., 1985). The presence of physical structures like upwelling fronts, eddies, river plumes and buoyancy-driven currents, among others, is considered to be a pre-requisite for most zooplankton aggregations (Franks, 1992; Shanks et al., 2000; Anderson et al., 2005; Vargas et al., 2006; Höfer et al.,

* Corresponding author.
E-mail addresses: j_weidberg@hotmail.com (N. Weidberg), angelika.renner@hi.no (A.H.H. Renner), sfp@akvaplan.niva.no (S. Falk-Petersen), sunnje.basedow@uit.no (S.L. Basedow).
[1] Present address: Department of Biological Sciences, University of South Carolina, 29208 Columbia, South Carolina, USA/Coastal Ecology Group, University of Vigo, 36310 Vigo, Spain.

https://doi.org/10.1016/j.jmarsys.2021.103697
Received 3 July 2021; Received in revised form 16 December 2021; Accepted 20 December 2021
Available online 24 December 2021

2015).

Nevertheless, spatial distributions of the largest and fastest zooplankters, like krill, can be effectively decoupled from the spatial patterns of environmental variables (Hamner et al., 1983; Ritz, 1997; Zhou and Dorland, 2004; Benoid-Bird et al., 2008; Krafft et al., 2012). Thus, it is possible that intrinsic biological features that cannot be inferred from the spatial distribution of environmental variables might affect zooplankton aggregations. The potential underestimation of the role of biological features in swarm formation led to statistical models that considered spatial autocorrelation to evaluate spatial patterns in ecological studies (Legendre and Fortin, 1989; Legendre, 1993). Combined with variance partitioning methods, these procedures allow to separate between spatial patterns of abundance associated with, or independent of, hydrographic structures (Legendre and Legendre, 1998; Belgrano et al., 1995; Lagos et al., 2008).

The copepod *Calanus finmarchicus* is a species well-suited to study the underlying mechanisms leading to large scale spatial aggregations. First, due to its high abundance and biomass in the pelagic ecosystems of the North Atlantic and Subarctic, this copepod is a key trophic link between primary producers and secondary consumers in these systems (Falk-Petersen et al., 2009; Melle et al., 2014). Secondly, in northern Norway there are historical observations of large surface concentrations (Sars, 1903; Bullen, 1913). Recently a large-scale swarm was detected by satellite imagery making it the first zooplankton species to be observed from the space (Basedow et al., 2019). The hydrography of the region where these large swarms are occurring is characterised by two major currents flowing in parallel towards the northeast: the cold and fresh Norwegian Coastal Current over the shelf and the warmer, more saline Norwegian Atlantic Current flowing along the continental slope (Sætre, 2007; Mork and Skagseth, 2010). The front and associated features between both currents, in combination with active organismal behaviours might provide retentive features for the copepods. Horizontal movements in calanoid copepods are limited in comparison with those of much larger and faster krill and mysids (Kils, 1982; Chen and Hwang, 2018), thus, the ability to form patches totally decoupled from environmental variables and driven solely by population dynamics may be low. Nevertheless, the location of deep overwintering habitats from which copepods emerge in early spring and to which they return in late summer could determine surface distributions regardless of spring-time hydrographic structures. Winter pre-conditioning is known to affect the spatial distributions of many pelagic species from phytoplankton to seabirds in spring (Schroeder et al., 2009; Black et al., 2010; Batchelder et al., 2013; Gonzalez-Gil et al., 2017). Overwintering habitats of *Calanus* spp. in the Norwegian Sea are mainly the Norwegian and Lofoten basins and to a lesser extent the deepest fjords along the coast (Halvorsen et al., 2003; Espinasse et al., 2016; Weidberg and Basedow, 2019).

In conjunction with a concurrent study focussed on patch detection based on ocean colour remote sensing (Basedow et al., 2019), our overall aim in this study is to delineate physical and biological effects on zooplankton swarm formation. For this, we sampled hydrography and spatial structures in detail at locations where copepod swarms are regularly indicated by ocean colour images. Our objectives are 1) to quantify the association of high copepod abundances with regional hydrographic structures, 2) to evaluate the role of spatial autocorrelation to detect biological factors driving copepod spatial distribution, 3) to investigate copepod vertical distribution across the patch, and 4) to infer and discuss the most likely mechanisms leading to patch formation as well as its dynamics under long-term, large-scale climatic forcing.

2. Material and methods

2.1. Study area

The northern Norwegian Sea off the Lofoten archipelago is characterised by a continental shelf that narrows towards the northeast, with widths of 95 km and 20 km off the sourthern and northern tips of the archipelago, respectively (Fig. 1). The Norwegian Coastal Current (NCC) flows on the shelf to the northeast, entering the Vestfjorden in between the islands and mainland Norway (Sætre, 2007). The NCC is formed by cold, fresh waters from the fjords and coastal areas. In spring, it is supplied by snow melt and forms then a wide wedge-shaped, shallow layer on top of the warmer, saltier Atlantic waters (Loeng, 1991; Sætre, 2007). Further offshore along the shelf break and over the Norwegian and the Lofoten Basins, the much saltier and warmer Norwegian Atlantic Current flows northeastwards.

The dominant mesozooplankton species in the region is *Calanus finmarchicus*. Copepodites stage V and adults ascend to surface waters at the onset of spring to feed on the phytoplankton bloom, which usually develops between February and April (Larsen et al., 2004). The following generation remains at the surface feeding and developing, until they reach copepodite stage IV-V in summer and then descend to depths around 1000 m to overwinter in a state of reduced metabolic activity called diapause (Hirche, 1996).

2.2. Field sampling

Data on the physical and biological environment were collected during a research cruise onboard R/V Helmer Hanssen from 28 April to 3 May 2017. Data were collected along four transects approximately orthogonal to the shelf break: two off the southern tip of the Lofoten archipelago on 28–29 April that were ca. 90 km long with a resulting angle of ca. 30° with respect to the east-west axis; and another two on 2–3 May across the narrow shelf break further northeast that were ca. 50 km long and with a resulting angle of 45° with respect to the east-west axis (Fig. 1). A Moving Vessel Profiler (MVP, Odim Brooke Ocean, Rolls Royce, Canada Ltd.) equipped with Conductivity Temperature Depth sensor (CTD, Seabird 19plusV2, Seabird Electronics Inc., USA), fluorescence sensor (F. WetLabs EcoFL, Seabird Electronics Inc., USA) and Laser Optical Plankton Counter (LOPC, Odim Brooke Ocean, Rolls Royce, Canada Ltd.) collected profiles down to ca. 800 m while the ship was moving along transects at a speed of 6–7 knots resulting in data with high spatial resolution. A 75 kHz RDI Ocean Surveyor Acoustic Doppler Current Profiler (ADCP) mounted on the drop keel of the boat was used to obtain cross-shelf profiles of current velocities.

In addition to the cross shelf transects, hydrographic conditions and zooplankton assemblages were measured at eight stations. Four stations were sampled around the southern transects in between 28 April and 1 May 2017; another four stations were sampled around the northern transects on 1–3 May (Table 1, Fig. 1).

2.3. Analyses of hydrography and water currents

Water mass distribution was analysed based on CTD data collected by the MVP along transects. Cross shore contour profiles were made with the software Surfer V8. In addition, vertical profiles of hydrography were obtained by a SeaBird 911plus CTD, which was deployed at each station to measure vertical profiles of temperature and salinity.

ADCP data were processed using a set of Matlab routines. This included calibration for misalignment of the transducer and signal amplitude, and derivation of absolute water velocities. To further reduce possible errors in water current estimates due to boat instabilities, measurements were averaged every 10 min. Then, a coordinate transformation was applied to current velocity with its eastern (u) and northern (v) component (angle $\Theta = 60$ and 45° with respect to the south-north line for southern and northern transects, respectively) to obtain along transect current as follows:

$$\text{Along transect current} = u^{*}sin(\Theta) - v^{*}\cos(\Theta) \quad (1)$$

Seaward currents along the transect will thus be negative, while landward currents will have a positive sign. To infer the role of tidal dynamics in the overall circulation observed along these transects,

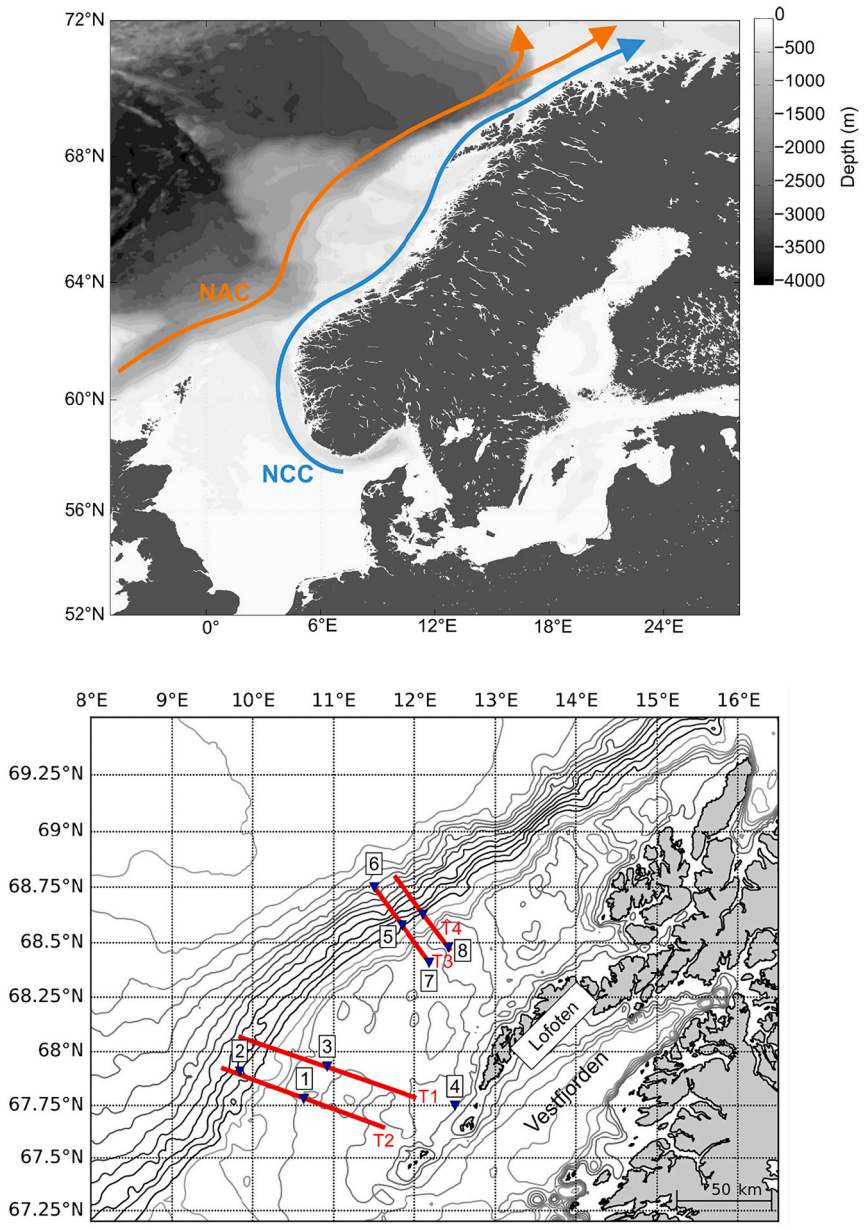

Fig. 1. Map of the region. The blue and orange arrows show the main pathways of the Norwegian Coastal Current (NCC) and the Norwegian Atlantic Current (NAC). Red lines mark the Moving Vessel Profiler (MVP) transects from T1 to T4. Inverted blue triangles and numbers from 1 to 8 show the position of the stations. Numbers for stations and transects were assigned following a temporal order. (For interpretation of the references to colour in this figure legend, the reader is referred to the web version of this article.)

Table 1
Characteristics of the stations sampled off the Lofoten archipelago.

Station	Day	Start time (UTC)	Region	Position	Latitude (°N)	Longitude (°E)	Depth (m)
1	28-april-17	10:56	South	Outer shelf	67.7810	10.6302	178
2	30-april-17	6:26	South	Off shelf	67.9076	9.8381	852
3	30-april-17	17:26	South	Outer shelf	67.9304	10.9282	182
4	01-may-17	1:05	South	Inner shelf	67.7461	12.5131	97
5	01-may-17	15:22	North	Off shelf	68.5790	11.8447	936
6	01-may-17	23:03	North	Off shelf	68.8333	11.4998	2183
7	02-may-17	15:27	North	Inner shelf	68.4104	12.1827	168
8	03-may-17	3:33	North	Inner shelf	68.4796	12.4206	151

hourly water heights above datum at Røsthavet (67.575°N, 12.439°E) were considered. These data were modelled from observations at Bodø (67.278°N, 14.366°E) and retrieved from 27 April to 4 May at the Norwegian Hydrographic Service website (https://www.kartverket.no/en/at-sea/se-havniva/).

2.4. Analyses of wind, upwelling and turbulence

Wind speed and direction were measured by a weather station mounted on the boat and saving data every minute. Time series of upwelling index were derived according to Bakun (1973)'s equation as:

$$UI = V*V_x*CD*\sigma_a*f^{-1}*\sigma_w{}^{-1} \quad (2)$$

where UI is the upwelling index in $m^3\ m^{-1}\ s^{-1}$, V is the wind velocity in m s^{-1}, V_x is the alongshore wind velocity in m s^{-1}, CD is the drag coefficient (0.0014), *f* is the Coriolis parameter (0.000168 at 68°N), σ_a is the air density (1.22 kg m^{-3}) and σ_w is the water density (1026.88 kg m^{-3}). This is the mean water density for the first 31 m of the water column calculated from the CTD dataset at the 8 stations sampled, as 31 m would the maximum depth for Ekman transport given the maximum wind speeds of 13 m s^{-1} recorded during the cruise (Pringle, 2007). Alongshore winds were calculated assuming an angle in between the east-west axis and the coast of 45°. The resulting upwelling index was multiplied by 1000 m to obtain the volume of water displaced offshore/onshore per km per second.

Turbulence was calculated according to the formulation in Pringle (2007) as:

$$E = V_t^{3} * k^{-1} \tag{3}$$

where E is the wind induced turbulence in watts * kg $^{-1}$at a depth of 1 m, V_t is the velocity scale in m s^{-1} of the turbulence approximated as one-thousandth of wind speed, and *k* is the von Kármán's constant (0.41).

2.5. Divergence and convergence based on satellite products

To infer divergence and convergence zones along the MVP transects, daily gridded sea level anomalies (SLA) with a spatial resolution of 0.25° were obtained from the AVISO delayed-time "allsat" product based on merged maps from all the satellites available at a given time (http://marine.copernicus.eu/services-portfolio/access-to-products/?option=com_csw&view=details&product_id=SEALEVEL_GLO_PHY_L4_REP_OBSERVATIONS_008_047). Analysis of SLA imagery has been applied to detect convergent/divergent areas at oceanic gyres (Sun et al., 2019).

2.6. Nutrients and chlorophyll a

At each station, water samples for nutrient analyses and chlorophyll *a* (chl *a*) filtration were sampled by Niskin bottles mounted on the CTD rosette frame at 0, 5, 10, 20 and 50 m for both parameters, and close to bottom for nutrients only. Nutrients were analysed at the university in Tromsø using standard sea water methods with a Flow Solution IV analyser (Becker et al., 2020). 50 to 150 ml of sea water from each bottle were filtered onto GF/C filters, which were frozen at −80 °C and subjected to chl *a* extraction with methanol and fluorometric measurements (Turner Designs fluorometer) in the laboratory.

Both fluorescence sensors, the one on the MVP and the one on the rosette frame at stations, were calibrated against chlorophyll *a* obtained from filtered water samples, resulting in regression lines of chl *a* = 0.0134* Fluorescence+0.0882 (r^2 = 0.6888; $P < 0.0001$) for the MVP sensor and chl *a* = 0.7975 * Fluorescence +0.2517 (r^2 = 0.6384; $P < 0.0001$) for the rosette sensor, respectively.

2.7. Analyses of C. finmarchicus. distribution

Mesozooplankton was sampled with a Multinet Midi (0.25 m^2, 180 μm, Hydrobios) at 5 depth strata: 0–2 m, 2–5 m, 5–30 m, 30–100 m, 100 m-bottom. Samples were preserved in a 4% formaline-seawater solution buffered with hexamine. Ashore, samples were analysed under the microscope to estimate the abundances of *C. finmarchicus*. Successive aliquots were analysed until at least 450 zooplankters and 100*C. finmarchicus* were counted.

The LOPC registers the flux of particles in between 0.1 and 25 mm and darker particles of 1–2 mm size were identified as *C. finmarchicus* CIV to adults (Basedow et al., 2014), based on earlier calibrations of the LOPC against Multinet and Video Plankton Recorder (Gaardsted et al., 2010; Basedow et al., 2013). Based on these data, the distribution of *C. finmarchicus* along transects was plotted and analysed with respect to physical parameters.

2.8. Statistical analyses of C. finmarchicus. swarms

Before examining factors influencing surface swarms in general, we performed statistical analyses of the vertical distribution of *C. finmarchicus* to test for environmental factors influencing surface occurrences. To examine variability in the vertical distribution of the copepods in the region, weighted mean copepod depths (WMD) were calculated for each downcast as follows:

$$\mathrm{WMD} = \sum \mathrm{N}^{*}\mathrm{D} \Big/ \left(\sum \mathrm{N} \right) \tag{4}$$

where N is the abundance of *C. finmarchicus*. CIV-adults in individuals m^{-3} (ind. m^{-3}), D is depth (m) and the summatories indicate sums across the water column at a given downcast. The predictor environmental variables included in the models for WMD were latitude, longitude, SLA, time of day to account for possible effects of diel vertical migration, chl *a* averaged for the first 10 m of the water column, and mixed layer depth (MLD) calculated as the depth at which a salinity gradient of 0.01 psu m^{-1} was attained (Wijesekera and Gregg, 1996). Such gradient thresholds are commonly used in mixed layer depth studies (Thomson and Fine, 2003).

To test for factors influencing *C. finmarchicus* swarms, the abundance of older stages (CIV to adults, ind. m^{-3}) was selected as dependent variable for the statistical models. Initially, longitude, latitude, water temperature, salinity, chl *a*, SLA and along transect currents were selected as environmental predictors. Temperature, salinity and depth were strongly correlated (Pearson's $R > 90\%$); we therefore decided to keep salinity as sole descriptor of water masses because it is the best proxy of the supply of snow melt to the Norwegian Coastal Current in spring. Thus, temperature was excluded from further analyses. Furthermore, we carried out all analyses for three depth strata: 0–5 m, 5–30 m, and 30–100 m. For each MVP downcast along the transects, copepod abundances and environmental variables were averaged over each of these depth layers.

Spatial autocorrelation is defined as a property by which nearby locations present values of an ecological variable (i.e. plankton concentrations) that significantly differ from those expected by chance (Legendre and Fortin, 1989; Legendre, 1993). Within a zooplankton swarm, spatial autocorrelation is positive as locations inside the patch are more similar among them than what could be expected from a random distribution. To account for spatial autocorrelation, a variance partitioning method was used. It consisted in developing three different kinds of models: a model including all environmental variables (ENV); a model including only spatial coordinates as predictors (latitude and longitude, SPA); and a model with all environmental variables and spatial coordinates as predictors (ENV + SPA). From these models, the three main components explaining variability in surface swarms can be separated: the one explained by the pure effect of environmental variables on the distribution of the organisms (*ENV*); the one explained by spatial autocorrelation effects not shared with any of the environmental variables (*SPA*); and the variability component due to the spatial structure of the environmental variables shared with the organismal distribution (*ENV:SPA*). These components can be extracted by subtracting the variance explained by each of the three kinds of models as follows:

$$ENV = (\mathrm{ENV} + \mathrm{SPA}) – \mathrm{SPA} \tag{5}$$

$$SPA = (\mathrm{ENV} + \mathrm{SPA}) – \mathrm{ENV} \tag{6}$$

$$ENV : SPA = (\mathrm{ENV} + \mathrm{SPA}) – (ENV + SPA) \tag{7}$$

This method has been applied to explain distributions of oribatid mites, coastal invertebrate recruitment rates, and planktonic distributions among others (Borcard et al., 1992; Belgrano et al., 1995; Lagos

et al., 2008; Ayata et al., 2011). The models implemented in these studies were General Linear Models (GLMs) for the environmental predictors and cubic polynomials for the spatial coordinates. Here, to account for non-linear relationships among variables, we used General Additive Mixed Models (GAMMs) with four knots for cubic splines fits and assuming a normal distribution of the dependent variable once square root-transformed. We inspected the linear fit of the normal probability plot for residuals to check the adequacy of the models (Wood., 2006). Their formulation was the following:

$$Y = \alpha + s\,(Y_1) + \ldots . s\,(Y_n) + \varepsilon \quad (8)$$

where Y is the dependent variable (copepod abundances at each depth strata and WMD, respectively), α is a constant, s is a smooth function applied to each of the predictors (Y_1 to Y_n) and ε is the error term. To account for the importance of each individual variable, we employed a stepwise backwards removal technique based on *p* values on the full ENV + SPA models to assign an amount of variability explained to each predictor.

3. Results

3.1. Hydrography and water currents

The main hydrographic structures in the region can be observed in the cross-shelf profiles obtained from the MVP transects (Fig. 2). Water with characteristics typical for the Norwegian Coastal Current occupied the upper 50 to 60 m along the southern two transects (T = 5–6 °C, S = 33.7–34). The presence of this coastal, colder and fresher waters along the two northern transects was less clear, with a low salinity layer roughly reaching 20 m deep at the coastal end of Transect 3, and a more mixed pattern along Transect 4. More saline and warmer water with characteristics of Atlantic Water occupied most of the water column. Off the shelf, cold Arctic waters with temperatures between −1 to 1 °C were observed below 600 m.

The hydrographic profiles sampled at the stations confirm the distribution of water masses observed by the MVP. Off the southern end of the Lofoten islands, hydrographic profiles at the stations show the clear cross shelf gradient (Fig. 3). Homogeneous low salinities and temperatures (Fig. 3D, S = 33.9, T = 5.5 °C) indicative of the Norwegian Coastal Current spanned over the whole water column at the inner shelf, while at the shelf break there was an intrusion of saltier and warmer Atlantic waters (Fig. 3B, E, S = 34.9, T = 7.5 °C) below 100 m deep. Off the shelf, these Atlantic waters occupied the upper 600 m, with colder Arctic waters (1 °C) below (Fig. 3F). To the northeast, on the shelf the presence of the low salinity surface layer was weaker, only at station 8 (Fig. 3H) surface waters reached low salinities around 33.9.

The cross shelf dynamic structure inferred from the along transect currents in the region was quite variable (Fig. 4A). In the south, strong onshore currents of 0.5 m s^{-1} were measured across the whole water column at the outer part of the shelf at Transect 1. Currents with opposite direction were measured at Transect 2. A similar reversal happened at the inner shelf, with offshore and onshore flows of 0.2 m s^{-1} at Transects 1 and 2, respectively. Off the shelf, offshore and onshore strong currents of 0.3–0.4 m s^{-1} were present at Transects 1 and 2, respectively. To the northeast, deep offshore and onshore currents of 0.4 m s^{-1} at 300–500 m developed off the shelf at Transects 3 and 4, respectively. On the northern shelf, currents of 0.25 m s^{-1} were directed offshore at Transect 3 and onshore at Transect 4. These reversals at adjacent transects were consistent with the tides, as Transects 1 and 2 were sampled at rising and falling spring tides, respectively (Fig. 4B). On the other hand, Transects 3 and 4 were sampled at falling and rising neap tides, respectively (Fig. 4B).

3.2. Wind, upwelling and turbulence

Wind dynamics were different among southern and northern transects (Fig. 5). Along Transect 1, winds were very weak, leading to slight upwelling and extremely low turbulence levels in the order of 10^{-7} W kg^{-1}. Upwelling increased to moderate southeasterly winds with a mean of 300 m^3 km^{-1} s^{-1}, and turbulence intensified (1.5 10^{-6} W kg^{-1}) along Transect 2. Along Transects 3 and 4, mean turbulence was around 2.5 10^{-6} W kg^{-1} with peaks of 4 10^{-6} W kg^{-1} due to northerly winds up to 10 m s^{-1}, and upwelling there reached almost 600 m^3 km^{-1} s^{-1}. A sharp transition to a mean downwelling of 200 m^3 km^{-1} s^{-1} was evident at the end of Transect 3 and beginning of Transect 4.

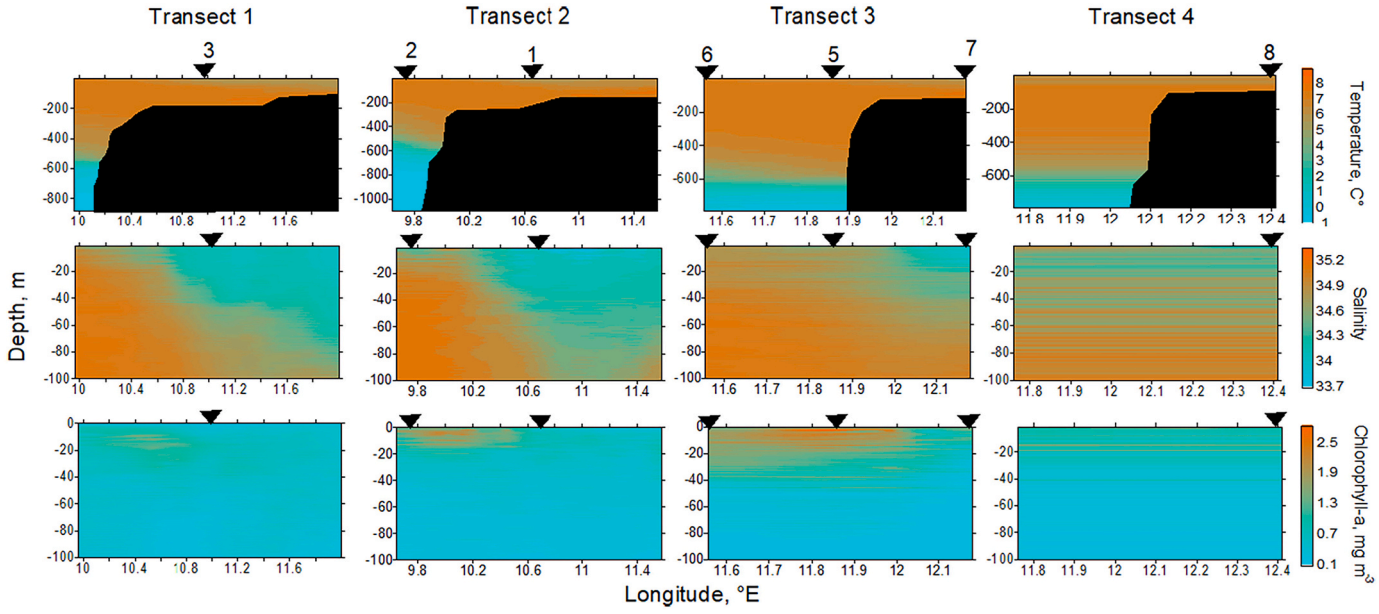

Fig. 2. Contour profiles of temperature, salinity and chl-a for the four MVP transects. For salinity and chl-a only the first 100 m of the water column are shown to better observe contrasting hydrographic structure. Inverted dark triangles mark the position of the stations, noted by numbers. Black areas indicate the bottom. (For interpretation of the references to colour in this figure legend, the reader is referred to the web version of this article.)

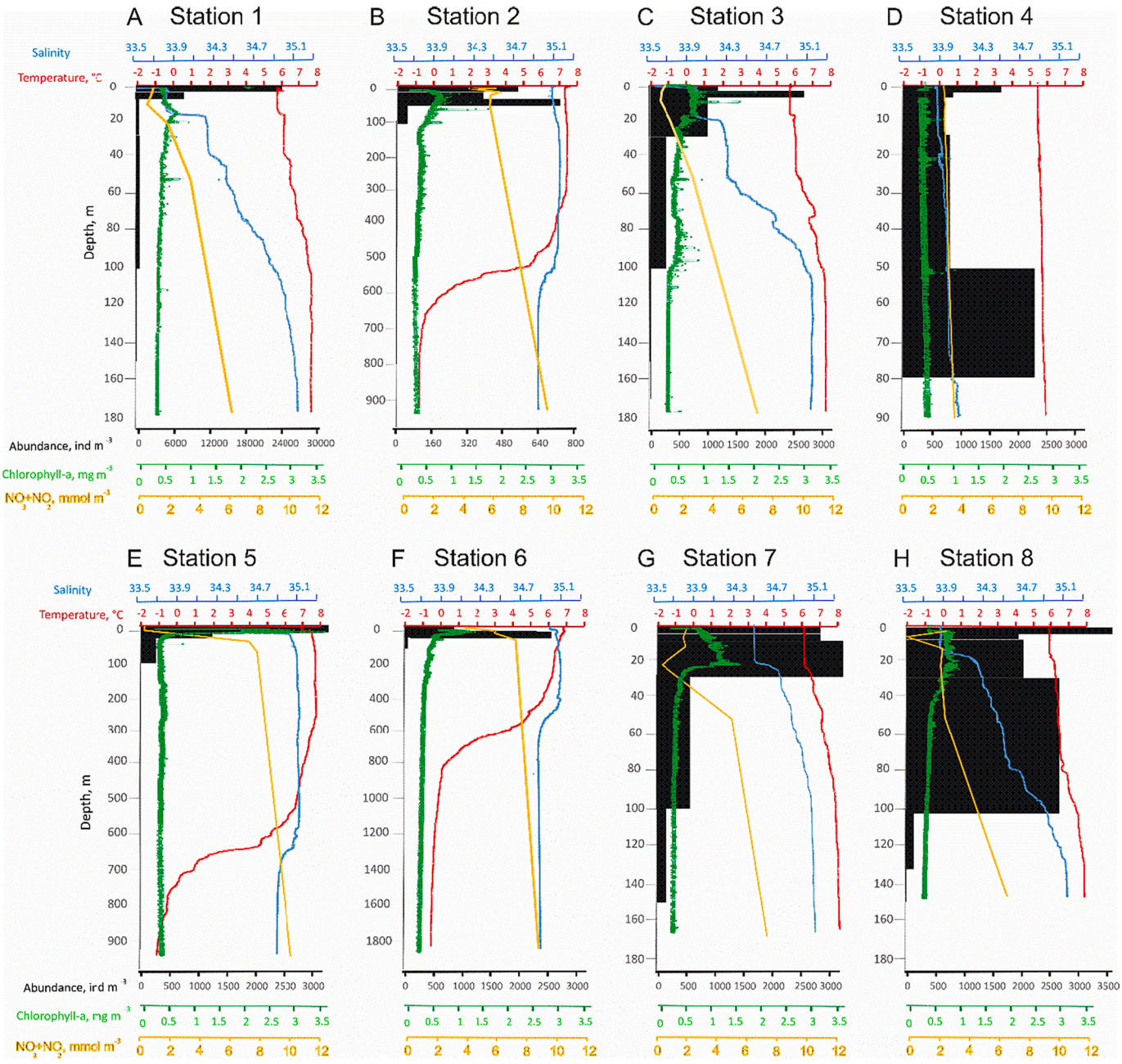

Fig. 3. Vertical profiles of temperature (red line), salinity (blue), chl-a (green), nutrients ($NO_3 + NO_2$, yellow) and copepod abundances from Multinet hauls (dark bars) at stations 1 to 8 (A to H). Ranges for X-axes are the same among panels for all the variables except for copepod abundances. (For interpretation of the references to colour in this figure legend, the reader is referred to the web version of this article.)

3.3. Nutrients and chlorophyll a

Partly depleted $NO_3 + NO_2$ concentrations between 0 and 6 mmol m^{-3} were measured in the upper 50 m, with higher concentrations offhelf in the northern area (Fig. 3). At the bottom, concentrations up to 11 mmol m^{-3} were observed off the shelf at the northern area at a depth of 950 m.

Along the southern MVP transects, chl *a* maximum concentrations around 2.5 mg m^{-3}, were measured offshore in the upper 20 m along parts of Transect 2 (Fig. 2). At Transect 2, subsurface maxima with concentrations around 1.5 mg m^{-3} were observed at the offshore end. To the north, higher concentrations around 3 mg m^{-3} were observed in surface waters at the shelf break (Transect 3), while subsurface maxima with lower values around 1.5 mg m^{-3} were observed along the entire Transect 4. Vertical profiles obtained at the stations show detailed distributions of chl *a* along the water column with peaks above 2 mg m^{-3} in the photic layer above 50 m and lower background values around 0.2–0.5 mg m^{-3} below (Fig. 3).

3.4. Distribution of Calanus finmarchicus

Overall, *C. finmarchicus* cross shelf distributions observed by the LOPC show clear aggregations in the epipelagic layer above 200 m (Fig. 6). Along the southern transects, the distribution was quite patchy (Fig. 6). Swarms with an approximate extension of 20 km and maximum abundances in the order of 10^4 ind. m^{-3} were found along the entire Transect 1. Along Transect 2, two large patches of 30–40 km in length and 100 m in depth were observed in the upper 100 m on top of the inner

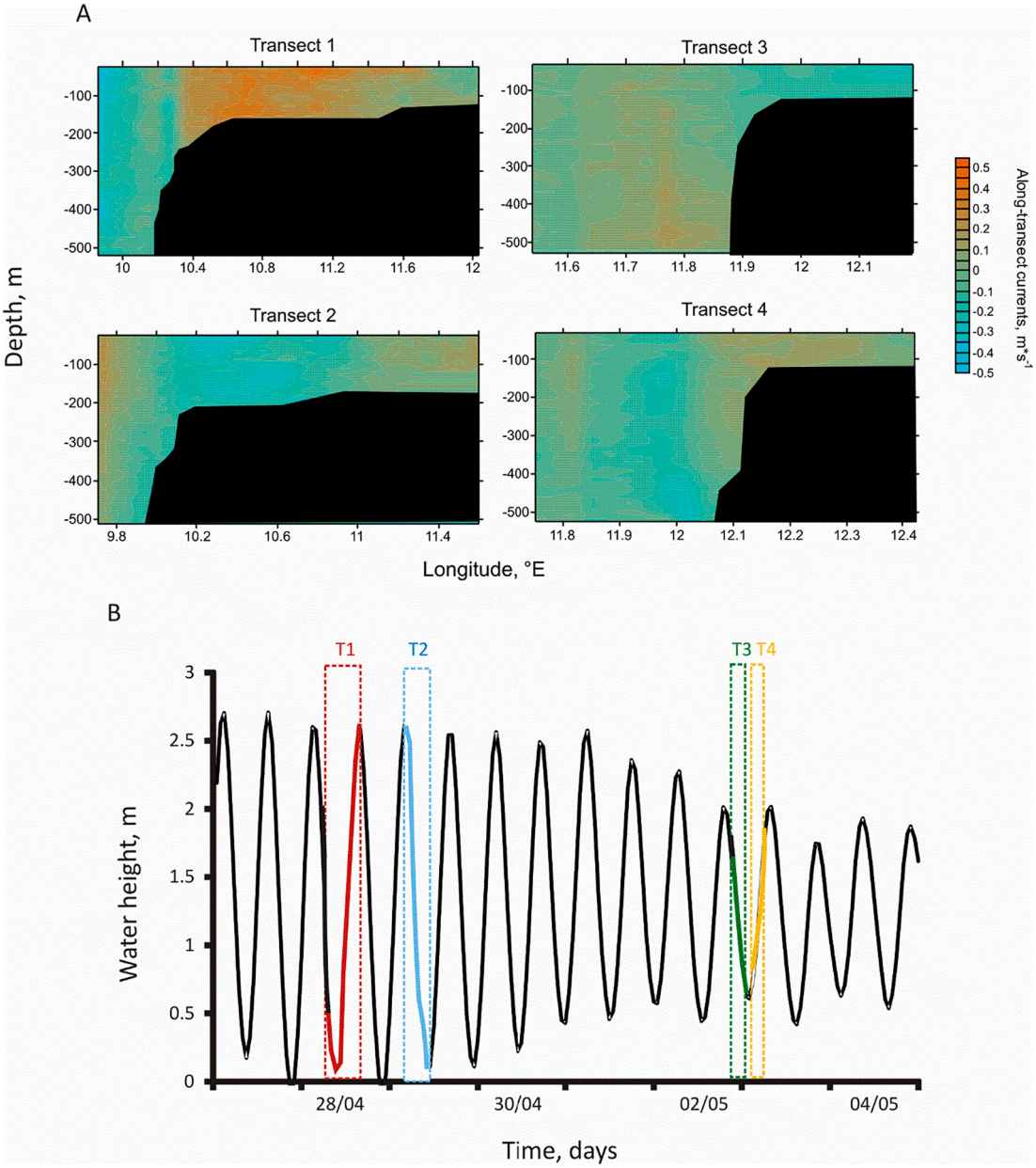

Fig. 4. A) Contour profiles of along transect currents for the four MVP transects. Positive and negative values point to landwards and seawards flows, respectively. B) Time series of water heights. Red, blue, green and yellow squares and lines show the time intervals at which transects 1 to 4 were sampled. (For interpretation of the references to colour in this figure legend, the reader is referred to the web version of this article.)

part of the shelf and at the shelf break. To the northeast, high abundances were observed on the shelf, extending over 20 to 30 km in length and partly occupying the entire water column above the shelf. Along all transects, generally low abundances were observed below 200 m but patches with up to 100 ind. m^{-3} did occur at these depths.

The vertical distribution of *C. finmarchicus* sampled by Multinet matched the patterns observed along the MVP transects, with most of the population within the first 100 m of the water column. In the southern region, abundances reached a maximum of 24,000 ind. m^{-3} in surface waters at the shelf break (Fig. 3). Abundances were very low below 100 m at these stations. Similarly, to the north highest copepod abundances were observed in the surface layer above 100 m with up to 3500 ind. m^{-3} (Fig. 3).

3.5. Factors influencing C. finmarchicus. swarms

The variance partitioning method based on the variability explained by the different GAMMs revealed the relative importance of three different components of variability in the spatial distributions of copepods (Fig. 7). Overall, total variability explained ranged from 38 to 57%, and the pure spatial component (*SPA*), which could not be explained by the distribution of any environmental variable, never exceeded 16%. The variability explained by the spatial distribution of the environmental predictors (*ENV:SPA*) was 16 and 6% for *C. finmarchicus* abundances in the 0–5 and 5–30 m depth layers, respectively, but increased to more than 29% for abundances in the 30–100 m layer. Also, the vertical distribution of the copepods, as indicated by their WMD, was explained to more than 30% by the spatial distribution of environmental predictors. The pure effect of the environment (*ENV*) on the abundance and distribution of copepods ranged

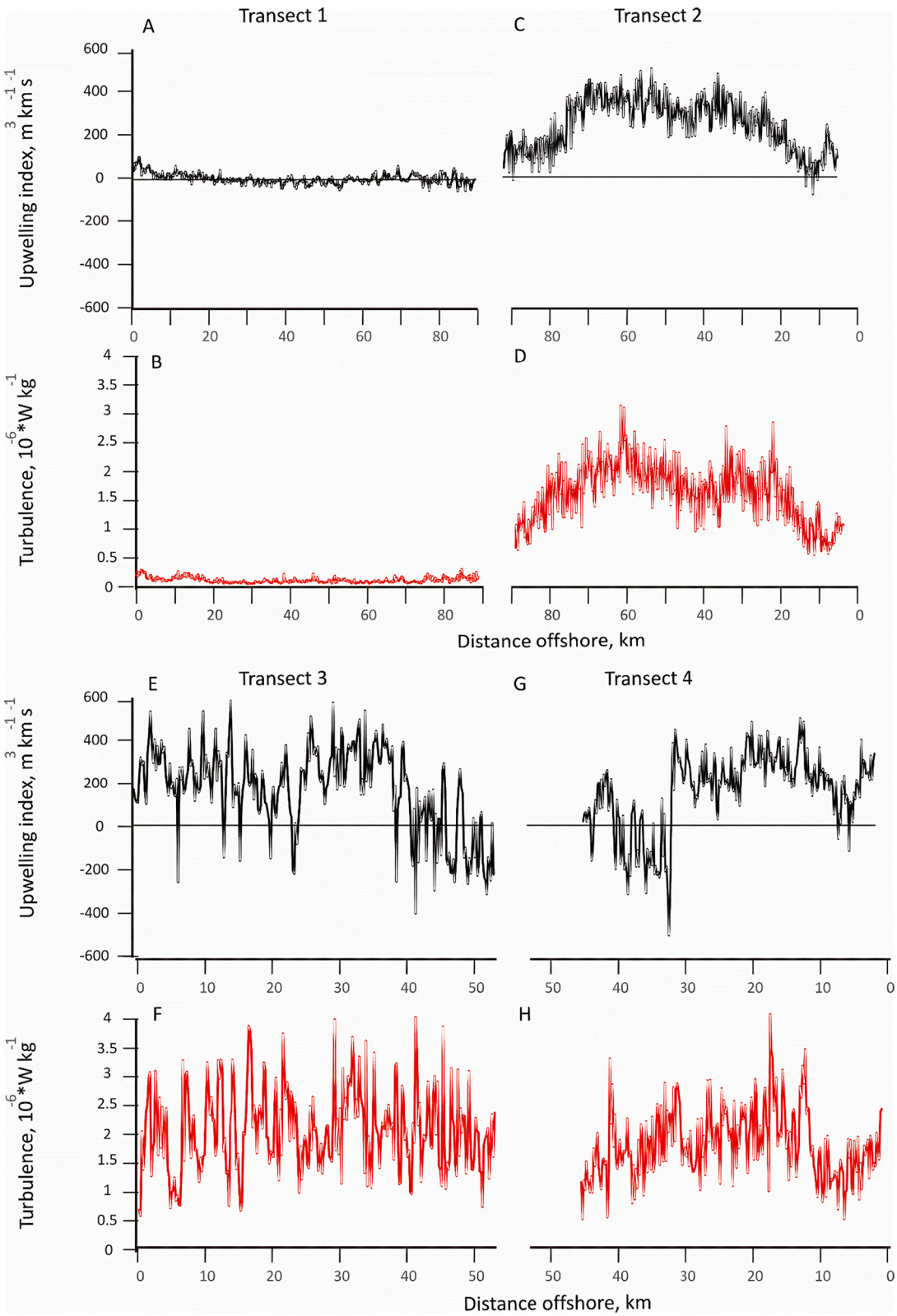

Fig. 5. Time series of wind derived upwelling (black lines) and turbulence (red lines) values along Transects 1, 2, 3 and 4 (A-B, C-D, E-F and G-H, respectively). For those transects started offshore (Transects 2 and 4), the x-axis was reversed to account for wind temporal variability. (For interpretation of the references to colour in this figure legend, the reader is referred to the web version of this article.)

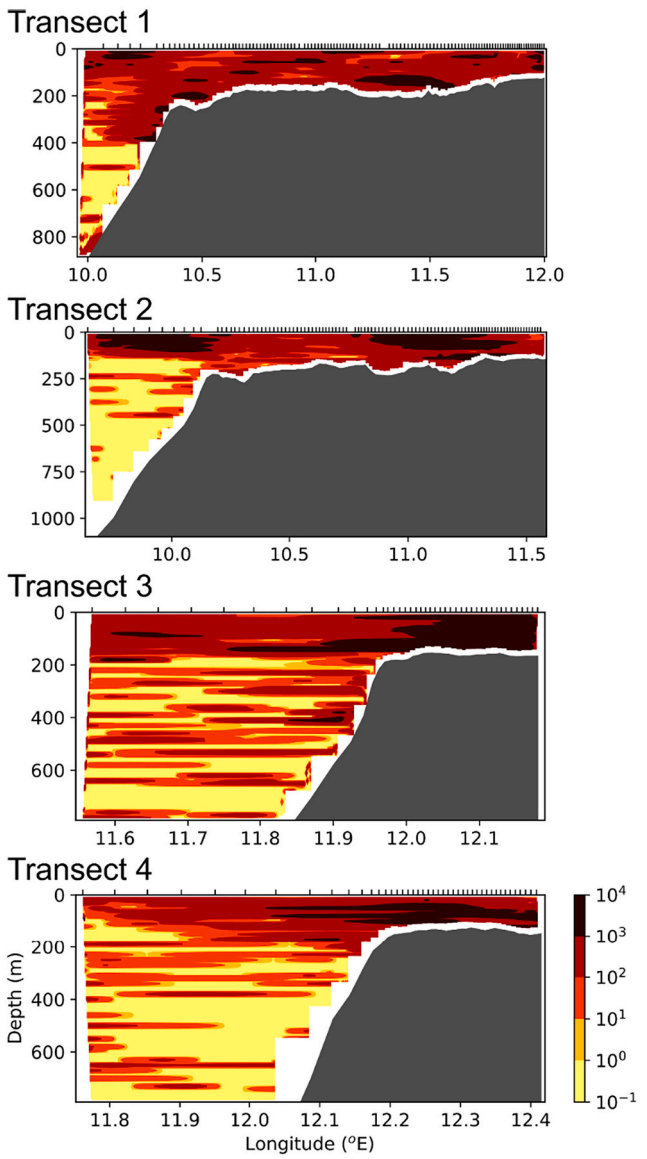

Fig. 6. Contour plots of *Calanus finmarchicus* abundances (individuals m^{-3}) along the four MVP transects. Abundances are represented in a logarithmic scale. Ticks in the upper horizontal axis show each LOPC downcast. (For interpretation of the references to colour in this figure legend, the reader is referred to the web version of this article.)

from 11% for WMD to 20% for the abundances in the 30–100 m depth layer. Considering *ENV* and *ENV:SPA* together as a proxy of the importance of environmental variables on spatial copepod assemblages, they accounted for a total from 23 to 54% of the variability in copepod distribution in the three layers and for 44% for WMD (Fig. 7).

Looking at the most relevant environmental variables in explaining *Calanus finmarchicus* vertical distribution and abundance revealed interesting connections (Fig. 8, Table 2). Copepod WMD was mostly affected by time of the day, with deeper vertical positions at midday indicative of a short range diel vertical migration with an amplitude around 10 m (Table 2, Fig. 8G). In addition, vertical positions were affected by SLA, as WMDs were shallower with increasing SLA (Table 2, Fig. 8H).

The most important effect on *C. finmarchicus* abundance at surface (0–5 m) was salinity: abundances markedly increased when salinity values dropped below 34.2 (Fig. 8, Table 2). This effect of salinity becomes statistically negligible at deeper layers (Table 2). Chl *a* had a positive effect on copepod abundances in this layer, with abundances increasing with increasing chl *a* concentration up to 1.5 mg m^{-3} and then flattening out. In the depth layer below the immediate surface, i.e. between 5 and 30 m, the most important predictor for copepod abundances was SLA: a negative association between higher abundances and low SLA estimates was observed (Table 2, Fig. 8). Also in this layer, there was a shift in the effect of chl *a* on copepod abundances, which turned to a negative association (Table 2, Fig. 8). Similar patterns were observed for the 30–100 m layer, where the same negative effect of SLA was the most important, while copepod abundances increased with seawards currents and low chl *a* concentrations (Table 2, Fig. 8).

4. Discussion

Extensive surface aggregations of *Calanus finmarchicus* were observed in spring 2017 off the Lofoten archipelago in the northern Norwegian Sea. They were associated with colder, less saline water layers corresponding to the Norwegian Coastal Current. In addition, the consistent negative effect at all depths of SLA on copepod abundances suggests that convergent zones characterised by downwelling are less favourable for aggregation. Although SLA also influenced copepod vertical distributions, this effect did not suppress a short range diel vertical migration. Abundances were typically higher in water masses flowing from the coast to oceanic areas. The effect of chl *a* was depth-dependent, with the positive relationship found in surface waters reversing at greater depths. Overall, aggregations responded mainly to the pure effect of hydrographic and hydrodynamic variables and their spatial structure in the region, suggesting that aggregations are highly susceptible to any environmental change acting on such structures.

4.1. Mechanisms of surface aggregations

The high abundances in the order of 10^4 ind. m^{-3} that we found have been previously recorded within the usual distribution range of *C. finmarchicus* in spring (Wishner et al., 1995; Planque et al., 1997; Nash and Geffen, 2004) and are also consistent with the size of overwintering populations off Northern Norway (Halvorsen et al., 2003; Weidberg and Basedow, 2019). These aggregations matched the spatial patterns observed in the satellite imagery obtained from a concurrent study, which was able to identify large reddish surface patches over the shelf (Basedow et al., 2019; Dong et al., 2021). Moreover, those images point to copepod swarms in areas typically influenced by coastal, cold, fresh waters from the Norwegian Coastal Current, as reddish surface areas included the shelf but also zones well into Vestfjorden (Basedow et al., 2019). This spatial match between the NCC and the swarm over such a large area observed in a weekly composite of satellite images indicates a consistent biophysical association. The important role of salinity in explaining copepod distributions at the very surface layer that we observed here also points to the interaction between the NCC and recently emerged copepods from overwintering as the main driver behind the formation of surface swarms (Fig. 8, Table 2).

The fact that aggregations occur over the shelf far from the main deep overwintering habitats at the Lofoten and Norwegian basins points to some role of horizontal advection in driving the accumulation process. We hypothesize that the NCC may act as an aggregation hotspot for offshore copepods. Surface plankton aggregations have been observed inside buoyant water masses like river plumes and have been explained by a mechanism called the “frog tongue” (Hetland et al., 2002). Essentially, surface planktonic populations would be overriden by the fast-moving buoyant plume because they cannot withstand downwelling flows at the plume front. Then, once the front has passed, upward swimming and/or buoyancy of the organism would drive plankton back to the surface, thus entering the plume. Such a mechanism has been observed around different buoyant water masses and has successfully explained planktonic cross shelf distributions (Vargas et al., 2006; Höfer et al., 2015; Höfer et al., 2017) but also spatial distribution of harmful

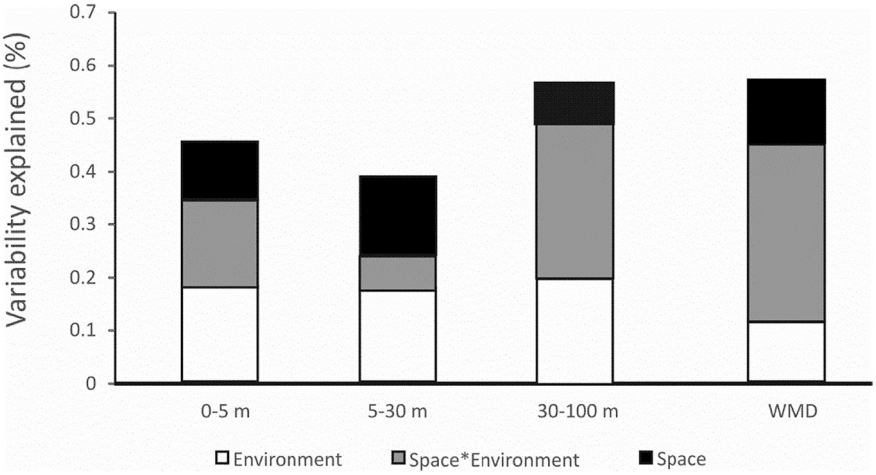

Fig. 7. Results of the variance partitioning method applied to copepod abundances at 3 different depth strata and copepod weighted mean depth.

algal blooms in the mesoscale around larger buoyancy driven currents (Franks and Anderson, 1992; McGyllicuddy et al., 2003; Anderson et al., 2005). In the particular scenario of northern Norway, the buoyant layer of the NCC would have to be displaced seawards to effectively override and trap recently ascended copepods off the shelf. Such offshelf movement usually occurs to the south around 63.5°N where the Halten Bank deflects a significant part of the NCC offshore to the shelf break (Sætre, 1999). In addition, offshore movements are typical in spring/summer when southwesterly winds drive the seawards spreading of the surface layer, thus making the characteristic wedge-shape of the NCC more conspicuous with a thinner surface layer (Sætre, 2007).

Another possible mechanism leading to copepod aggregations within the NCC is that the buoyant surface layer may act as a retentive feature for those copepods that overwintered in deep fjords. In spring typical estuarine circulation develops in these fjords causing surface offshore export of recently ascended copepods and euphausids (Zhou et al., 2005; Espinasse et al., 2016; Espinasse et al., 2018). Once over the shelf, the front between the NCC and Atlantic Waters could be an effective barrier for offshelf transport, thus enhancing aggregations within the NCC (Dong et al., 2021). It is unclear if overwintering populations in the deep fjords would be large enough to substantially contribute to a large swarm over the shelf, although in Vestfjorden high wintertime copepod concentrations in the same order as those found in the Lofoten Basin have been observed (Espinasse et al., 2016; Weidberg and Basedow, 2019). Nevertheless, this retention mechanism and the cross-shelf entrainment of offshore populations are not mutually exclusive and both can be operating simultaneously to form a large surface shelf patch.

Despite of the potential source of copepods, if these buoyant water masses affect copepod distributions, then the wind induced weakening of the surface density structure may cause dissipation of the patch, at least on a local scale, as shown in modelling studies (Fong and Geyer, 2001; Skagseth et al., 2011). Consistently, our results suggest that copepod abundances were in general lower to the north (Figs. 3, 6) where the buoyant surface layer was much weaker compared to the southern transects (Fig. 2) and winds were blowing stronger (Fig. 5).

The role of behaviour in the formation of the swarms within the buoyant NCC is relevant as aggregations will not happen if animals do not stay in the surface layer. To remain there, it is possible that the lipid sac that drives upward vertical migration contributes to keep the animals floating. Accordingly, experiments performed with *C. finmarchicus* from Loch Etive show that conspicuous surface aggregations occurred as surface salinity and in turn the density contrast between the animal and the water increased (Cohen et al., 2019). In contrast, our results show that copepod abundances increased at surface low salinity waters. Nevertheless, salinity values representative of Loch Etive (24–34) barely overlapped with those observed off the Lofoten Archipelago during our cruise (33.7–35.2), thus preventing any valuable comparison. On the other hand, calanoid copepods can stay at the surface by actively swimming upwards, even against downwelling currents up to 2 cm * s^{-1} (Weidberg et al., 2021).

4.2. *Vertical distributions and processes*

The persistent negative effect of SLA on copepod abundances for the three depth layers points to a clear effect of vertical water motion on plankton distribution in the region. Such an effect is consistent with Ekman transport dynamics in the open ocean, circulation in oceanic gyres and large-scale climatic forcing. All these processes create divergent and convergent surface areas with lower and higher SLA, respectively (Pond et al., 1983; Ruiz Etcheverry et al., 2016). In turn, to balance the difference in surface height, opposite vertical motions develop, with upwelling at divergences and downwelling at convergences. Our results suggest that copepods accumulated at regions where SLA was close to 0, an intermediate condition between downwelling and upwelling. (Fig. 8). Thus, the negative effect of SLA on copepod abundances may reflect aggregations at regions with reduced vertical motions. Similarly, subsurface aggregations of mysids were observed only when vertical currents were close to zero across a small fjord at the American Pacific coast (McManus, 2003). Reduced vertical water motion might allow copepods to ascend into surface waters more easily. On the other hand, horizontal cross shore currents influence copepod distributions at waters below 30 m, with higher abundances found at water masses flowing offshore (Fig. 8F). Offshore advection could be beneficial for copepods at this deeper layer, as probably these belong to the first generation already descending to diapause (Hirche, 1996; Häfker et al., 2018). Such cross shore transport would probably be coupled to tides, as the current reversals we observed at adjacent transects match remarkably well shifts in tidal phases (Fig. 4B). Accordingly, strong semidiurnal and diurnal tidal currents have been observed in different shelf areas of the Norwegian Sea (Moe et al., 2003; Skarðhamar et al., 2015).

Time of the day was the most important predictor driving copepod WMD (Table 2), which clearly indicates synchronised diel vertical migration. We found a consistent although short-range deepening of WMD at midday (Fig. 8), even though day length was 18 h at the time of the cruise. Most likely, the persistence and amplitude of diel vertical migration does not only depend on photoperiod but is finely tuned by complex trade-offs in between surface food availability and higher potential mortality by UV-driven damage and predation (Cisewski et al., 2010; Wallace et al., 2010; Darnis et al., 2017).

Vertical position of copepod populations can impact the structure of pelagic food webs and our results suggest that their trophic impact may

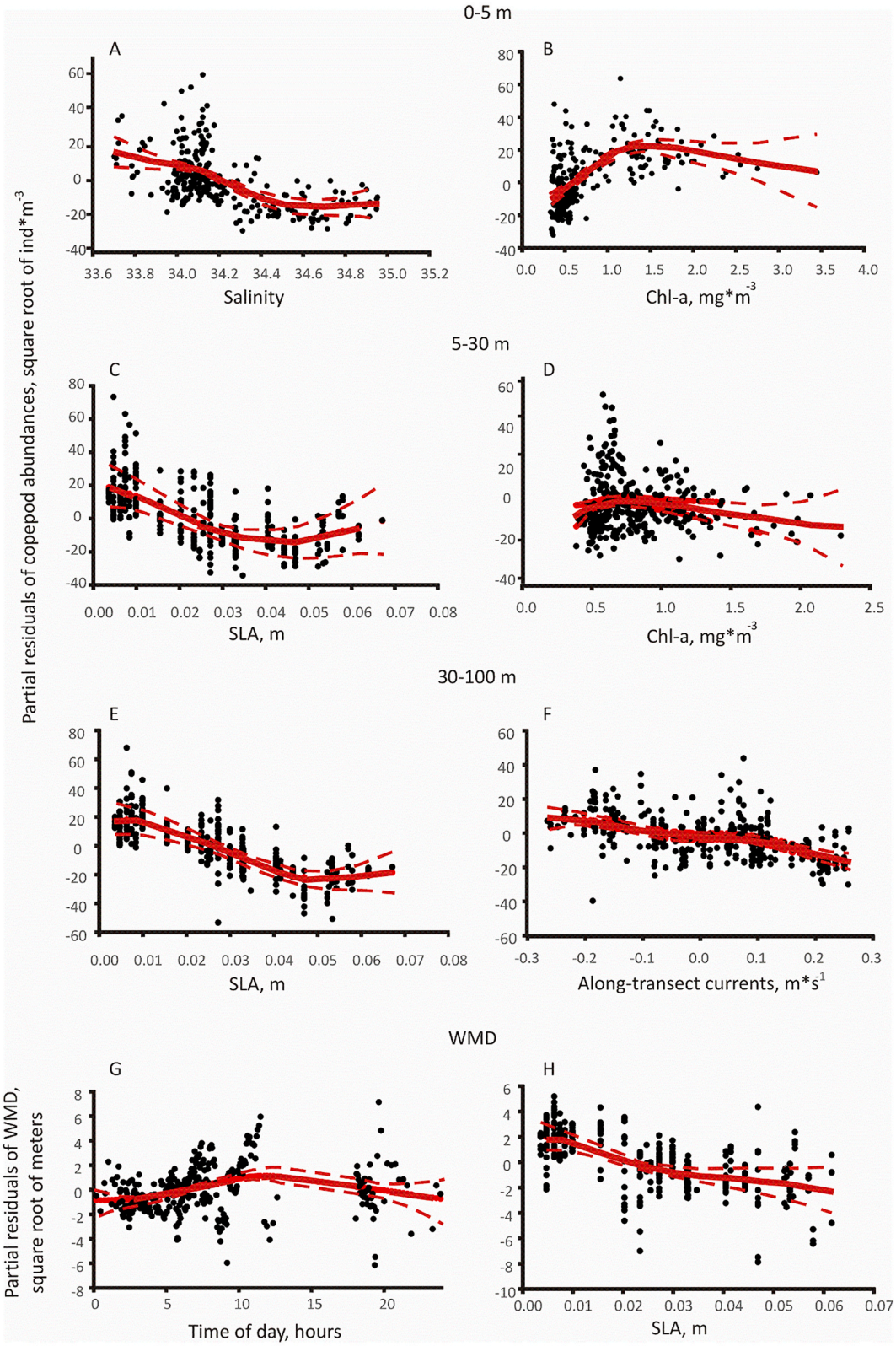

Fig. 8. Effects of the most important environmental variables on copepod abundances at 0–5 m (A-B), 5–30 m (C-D) 30–100 m (*E*-F) and WMD (G-H) obtained through the backwards removal technique on the full ENV + SPA GAMMs. Red lines showed the GAMM fits to partial residuals of each dependent variable, including 95% confidence intervals with discontinuous lines. (For interpretation of the references to colour in this figure legend, the reader is referred to the web version of this article.)

Table 2
Results of the full ENV + SPA GAMMs for each individual variable.

	Abundance 0_5m	Abundance 5_30m	Abundance 30_100m	WMD
Latitude	0.0234*	0.1331 ***	0.1946***	0.0930**
Longitude	0.1291**	0.0866***	0.1794***	0.0562***
Salinity	0.1606***	0.0324 n.s.	0.0108 n.s.	
CHLA	0.1341***	0.0368**	0.0330**	
SLA	0.014***	0.0614***	0.1021***	0.0324***
Along-transect current		0.0346**	0.0534**	
CHLA_10m				0.0167*
MLD				0.0179*
Time of day				0.3558***

Variance explained is shown together with significance level (n.s.: non significant; *:0.05 > p > 0.01; **:0.01 > p > 0.001; ***:0.001 > p).

change with depth. There was a strong positive effect of chl *a* concentrations on copepod abundances in the first 5 m of the water column, but at deeper layers this association weakened and turned negative (Fig. 8, Table 2). We hypothesize that such a shift was due to a depth-related change in the trophic dynamics between phytoplankton and copepods. In the Norwegian Sea, phytoplankton populations at the end of winter are thought to be controlled by recently emerged *C. finmarchicus* and other non- overwintering copepod species (Bathman et al., 1990). However, at the surface, high phytoplankton growth rates in early spring driven by relatively high nutrient concentrations and increasing light may overcome copepod grazing rates. Chl *a* concentrations peaked in the surface layer sustained by $NO_3 + NO_2$ concentrations that, although lower than at greater depths, are far from being completely depleted (Fig. 3). In deeper layers, higher nutrient concentrations around 10 mmols m^{-3} were similar to winter maximum values (Reigstad et al., 2002), but light becomes the limiting factor for phytoplankton growth. In this scenario copepod grazing rates can effectively control primary productivity. Accordingly, grazing rates of calanoids were observed to exceed primary productivity below 50 m depth in the Barents Sea (Eilertsen et al., 1989).

4.3. Resilience of patch spatial structure

The spatial distribution of the environmental variables (*ENV:SPA*) and their pure effect (*ENV*) were the more important correlates of copepod distribution (Fig. 7). Similar results highlighting the role of the spatial patterns of environmental predictors have been obtained from studies on the distribution of plankton (Belgrano et al., 1995; Ayata et al., 2011) but also of other organisms in the marine and terrestrial realms (van Rensburg et al., 2002; Astorga et al., 2003; Lagos et al., 2008). Thus, the variables used as potential descriptors of copepod distribution in our study contributed substantially to reduce *SPA*, the pure spatial effect which could only be explained by geographic coordinates. Such a minor effect of *SPA* suggests that intrinsic spatial autocorrelation effects not related to environmental forcing, have little importance. Consequently, spatial assemblages of copepods could be forecasted by inferring the spatial distribution of the main hydrographic features in the region. However, this also means that they may be highly susceptible to long term climatic shifts. In particular, as freshwater discharges become more dependent on winter rainfall than on spring snowmelt with global warming (Hanssen-Bauer et al., 2015; Vormoor et al., 2016), temporal mismatches between the formation of the buoyant surface layer of the NCC, the phytoplankton blooms and the emergence of overwintering copepod populations could occur (Bagøien et al., 2012).

5. Conclusions

Large scale aggregations were found to be clearly associated with the buoyant surface layer of the NCC over the shelf, which probably accumulated copepods from both the overwintering habitats on the Norwegian and Lofoten Basins and from the deepest fjords along the coast. Deeper in the water column, higher copepod abundances were clearly associated with reduced sea level anomalies, which suggest the occurrence of aggregations at regions with low vertical advection. Short range diel vertical migrations of the population were observed, despite the sun being above the horizon for >18 h each day. The *C. finmarchicus* patches were strongly linked to spatial hydrographic structures, and might be predicted but also highly impacted by large scale climatic forcing acting on onshelf water masses.

Declaration of Competing Interest

The authors declare that they have no known competing financial interests or personal relationships that could have appeared to influence the work reported in this paper.

Acknowledgements

We thank captain and crew of R/V “Helmer Hanssen” and the engineers of UiT. This study is part of the project “Sustainable harvesting of a patchy resource: aggregation mechanisms and implications for stock size estimates (Sea Patches)” that was supported by the Norwegian Research Council (grant number 268391/E40). During data processing and manuscript elaboration, N. Weidberg was funded by NASA grant 80NSSC20K0074.

References

Anderson, D.M., Keafer, B.A., Geyer, W.R., Signell, R.P., Loder, T.C., 2005. Toxic Alexandrium blooms in the western gulf of Maine: the plume advection hypothesis revisited. Limnol. Oceanogr. 50 (1), 328–345.
Astorga, A., Fernández, M., Boschi, M., Lagos, N.A., 2003. Two oceans, two taxa and one mode of development: latitudinal diversity patterns of south American crabs and test for possible causal processes. Ecol. Lett. 6, 420–427.
Ayata, S.D., Stolba, R., Comtet, T., Thiébaut, É., 2011. Meroplankton distribution and its relationship to coastal mesoscale hydrological structure in the northern Bay of Biscay (NE Atlantic). J. Plankton Res. 338, 1193–1211.
Bagøien, E., Melle, W., Kaartvedt, S., 2012. Seasonal development of mixed layer depths, nutrients, chlorophyll and *Calanus finmarchicus* in the Norwegian Sea – a basin-scale habitat comparison. Prog. Oceanogr. 103, 58–79.
Bakun, A., 1973. Coastal upwelling indices, west coast of North America, 1946-1971 U.S. Deptartment of Commerce, NOAA Technical Report.
Basedow, S.L., Tande, K.S., Norrbin, M.F., Kristiansen, S., S., 2013. Capturing quantitative zooplankton information in the sea: performance test of laser optical plankton counter and video plankton recorder in a *Calanus finmarchicus* dominated summer situation. Prog. Oceanogr. 108, 72–80. https://doi.org/10.1016/j.pocean.2012.10.005.
Basedow, S.L., Zhou, M., M., and K. S. Tande., 2014. Secondary production at the polar front, Barents Sea, august 2007. J. Mar. Syst. 130, 147–159. https://doi.org/10.1016/j.jmarsys.2013.07.015.
Basedow, S.L., McKee, D., Lefering, I., Gislason, A., Daase, M., Trudnowska, E., Falk-Petersen, S., 2019. Remote sensing of zooplankton swarms. Sci. Rep. 9 (1), 686. https://doi.org/10.1038/s41598-018-37129-x.
Batchelder, H.P., Daly, K.L., Davis, C.S., Ji, R., Ohman, M.D., Peterson, W.T., Runge, J.A., 2013. Climate impacts on zooplankton population dynamics in coastal marine ecosystems. Oceanogr. 26 (4), 34–51. https://doi.org/10.5670/oceanog.2013.74.
Bathman, U.V., Noji, T.T., von Bodungen, B., 1990. Copepod grazing potential in late winter in the Norwegian Sea - a factor in the control of spring phytoplankton growth? Mar. Ecol. Prog. Ser. 60, 225–233.
Becker, S., Aoyama, M., Woodward, E., Malcolm, S., Bakker, K., Coverly, S., Mahaffey, C., Tanhua, T., 2020. Repeat hydrography nutrient manual: the precise and accurate determination of dissolved inorganic nutrients in aeawater, using continuous flow analysis methods. Front. Mar. Sci. 7 (908).
Belgrano, A., Legendre, P., Dewarumez, J., 1995. Spatial structure and ecological variations of meroplankton on the French-Belgian coast of the North Sea. Mar. Ecol. Prog. Ser. 128, 43–50.
Benoid-Bird, K.J., Zirbel, M.J., McManus, M.A., 2008. Diel variation of zooplankton distributions in Hawaiian waters favors horizontal diel migration by midwater micronekton. Mar. Ecol. Prog. Ser. 367, 109–123.
Black, B.A., Schroeder, I.D., Sydeman, W.J., Bograd, S.J., Lawson, P.W., 2010. Wintertime Ocean conditions synchronize rockfish growth and seabird reproduction in the Central California current ecosystem. Can. J. Fish. Aquat. Sci. 67, 1149–1158. https://doi.org/10.1139/F10-055.
Borcard, D., Legendre, P., Drapeau, P., 1992. Partialling out the spatial component of ecological variation. Ecology 73, 1045–1055.
Bullen, G.E., 1913. Mackerel and Calanus. Nature 91, 531.

Chen, M.R., Hwang, J.S., 2018. The swimming behavior of the calanoid copepod *Calanus sinicus* under different food concentrations. Zool. Stud. 57, 13. https://doi.org/10.6620/ZS.2018.57-13.
Cisewski, B., Strass, V.H., Rhein, M., Krägefsky, S., 2010. Seasonal variation of diel vertical migration of zooplankton from ADCP backscatter time series data in the Lazarev Sea, Antarctica. Deep-Sea Res. 57, 78–94.
Cohen, J.H., Last, K., Waldie, J., Pond, D.W., 2019. Loss of buoyancy control in the copepod *C. finmarchicus*. J. Plankton Res. 41 (5), 787–790.
Darnis, G., et al., 2017. From polar night to midnight sun: diel vertical migration, metabolism and biogeochemical role of zooplankton in a high Arctic fjord (Kongsfjorden, Svalbard). Limnol. Oceanogr. 62, 1586–1605.
Dong, H., Zhou, M., Hu, Z., Zhang, Z., Basedow, S.L., Smith Jr., W.O., 2021. Transport barriers and the retention of *Calanus finmarchicus* on the Lofoten shelf. J. Geophys. Res. Oceans. https://doi.org/10.1029/2021JC017408.
Eilertsen, H.C., Tande, K.S., Taasen, J.P., 1989. Vertical distributions of primary production and grazing by *Calanus glacialis* Jaschnov and *C. hyperboreus* Kroyer in Arctic waters (Barents Sea). Polar Biol. 9, 253–260.
Espinasse, B., Basedow, S.L., Tverberg, V., Hattermann, T., Eiane, K., 2016. A major *Calanus finmarchicus* overwintering population inside a deep fjord in northern Norway: implications for cod larvae recruitment success. J. Plankton Res. 38 (3), 604–609. https://doi.org/10.1093/plank t/fbw024.
Espinasse, B., Tverberg, V., Kristensen, J.A., Skreslet, S., Eiane, K., 2018. Winter mortality in Calanus populations in two northern Norwegian fjords from 1984 to 2016. Polar Biol. https://doi.org/10.1007/s00300-018-2294-5.
Falk-Petersen, S., Hopkins, C.C.E., 1981. Zooplankton sound scattering layers in north Norwegian fjords: interactions between fish and krill shoals in a winter situation in Ullsfjorden and Øksfjorden. Kieler Meeresforsch. Sonderh. 5, 191–201.
Falk-Petersen, S., Mayzaud, P., Kattner, G., Sargent, J., 2009. Lipids and life strategy of Arctic. Calanus. Mar. Biol. Res. 5, 18–39. https://doi.org/10.1080/17451000802512267.
Fasham, M.J.R., 1978. The statistical and mathematical analysis of plankton patchiness. Oceanogr. Mar. BioI. Ann. Rev. 16, 43–79.
Folt, C.L., Burns, C.W., C.W., 1999. Biological drivers of zooplankton patchiness. Trends Ecol. Evol. 14 (8), 300–305.
Fong, D.A., Geyer, W.R., 2001. Response of a river plume during an upwelling favorable wind event. J. Geophys. Res. 196, 1067–1084.
Fornshell, J.A., Tesei, A., 2013. The development of sonar as a tool in marine biological research in the XXth century. Int. J. Oceanogr. 672621, 1–9.
Franks, P.J.S., 1992. Sink or swim: aggregation of biomass at fronts. Mar. Ecol. Prog. Ser. 82, 1–12.
Franks, P.J.S., Anderson, D.M., 1992. Alongshore transport of a toxic phytoplankton bloom in a buoyancy current: *Alexandrium tamarense* in the Gulf of Maine. Mar. Biol. 112, 153–164.
Gaardsted, F., Tande, K.S., Basedow, S.L., 2010. Measuring copepod abundance in deep-water winter habitats in the NE Norwegian Sea: Intercomparison of results from laser optical plankton counter and multinet. Fish. Oceanogr. 19, 480–492.
Genin, A., Jaffe, S.J., Reef, R., Richter, C., Franks, P.J.S., 2005. Swimming against the flow: a mechanism of zooplankton aggregation. Science 308, 860–862.
Gonzalez-Gil, R., Gonzalez-Taboada, F., Caceres, C., Largier, J.L., Anadon, R., 2017. Winter-mixing preconditioning of the spring phytoplankton bloom in the Bay of Biscay. Limnol. Oceanogr. 63, 1264–1282.
Häfker, N.S., Teschke, M., Last, K.S., Pond, D.W., Hüppe, L., Meyer, B., 2018. *Calanus finmarchicus* seasonal cycle and diapause in relation to gene expression, physiology, and endogenous clocks. Limnol. Oceanogr. 63 (6), 2815–2838.
Halvorsen, E., Tande, K.S., Edvardsen, A., Slagstad, D., Pedersen, O.P., 2003. Habitat selection of overwintering *Calanus finmarchicus* in the NE Norwegian Sea and shelf waters off northern Norway in 2000–02. Fish. Oceanogr. 12, 339–351.
Hamner, W.M., Hamner, P.P., Strand, S.W., Gilmer, R.W., 1983. Behaviour of Antarctic krill, *Euphausia superba*: chemo -reception, feeding, schooling, and molting. Science 220, 433–435.
Hanssen-Bauer, I., et al., 2015. Klima i Norge 2100 – Kunnskapsgrunnlag for klilmatilpasning oppdatert i 2015 (Climate in Norway 2100 – Science Basis for Climate Adaption Updated in 2015). NCCS report no. 2/2015.
Hardy, A.C., Gunther, E.R., 1935. The plankton of the South Georgia whaling grounds and adjacent waters, 1926-1927. Discov. Rep. II, 1–456.
Haury, L.R., McGowan, J.A., Wiebe, P.H., 1978. Patterns and processes in the time-space scales of plankton distributions. In: Steele, H. (Ed.), Spatial Pattern in Plankton Communities. Plenum, New York, pp. 277–327.
Hetland, R.D., McGyllicuddy, D.J., Signell, R.P., 2002. Cross-frontal entrainment of plankton into a buoyant plume: the frog tongue mechanism. J. Mar. Res. 60, 763–777.
Hirche, H.J., 1996. Diapause in the marine copepod, *Calanus finmarchicus* — a review. Ophelia 44 (1–3), 129–143.
Höfer, J., Weidberg, N., Molina-Ramirez, A., Cañas-Rueda, A., Garcia-Florez, L., Fernandez-Rueda, M.P., Acuña, J.L., 2015. Small-scale effects of a river plume front on the distribution of salps and doliolids. J. Plankton Res. 37, 1166–1180.
Höfer, J., Muñiz, C., Weidberg, N., Garcia-Florez, L., Acuña, J.L., 2017. High densities of stalked barnacle larvae (Pollicipes pollicipes) inside a river plume. J. Plankton Res. 39 (2), 316–329.
Kils, U., 1982. Swimming Behavior, Swimming Performance and Energy Balance of Antarctic Krill *Euphausia superba*. PhD thesis. University of Kiel. BIOMASS Scientific Series 3, BIOMASS Research Series.
Krafft, B.A., Skaret, G., Knutsen, T., Melle, W., Klevjer, T., Søiland, H., 2012. Antarctic krill swarm characteristics in the Southeast Atlantic sector of the Southern Ocean. Mar. Ecol. Prog. Ser. 465, 69–83.
Krause, J., Ruxton, G.D., 2002. Living in groups. Oxford University Press, Oxford. https://doi.org/10.1038/091531a0.
Lagos, N.A., Castilla, J.C., Broitman, B.R., 2008. Spatial environmental correlates of intertidal recruitment: a test using barnacles in northern Chile. Ecol. Monogr. 782, 245–261.
Larsen, A., Flaten, G.A.F., Sandaa, R.A., Castberg, T., Thyrhaug, R., Erga, S.R., Jacquet, S., Bratbak, G., 2004. Spring phytoplankton bloom dynamics in Norwegian coastal waters: microbial community succession and diversity. Limnol. Oceanogr. 49, 180–190.
Legendre, P., 1993. Spatial autocorrelation: trouble or new paradigm? Ecology 74, 1659–1673.
Legendre, P., Fortin, M.J., 1989. Spatial pattern and ecological analysis. Vegatatio 80, 107–138.
Legendre, P., Legendre, M., 1998. Numerical Ecology, 2nd edition. Elsevier Science BV, Amsterdam.
Loeng, H., 1991. Features of the physical oceanographic conditions of the Barents Sea. Polar Res. 10, 5–18.
Mackas, D.L., Denman, K.L., Abbot, M.R., 1985. Plankton patchiness: biology in the physical vermacular. Biol. Bull. Mar. Sci. 37 (2), 654–674.
McGyllicuddy, D.J., Signell, R.P., Stock, C.A., Keafer, B.A., Keller, M.D., Hetland, R.D., Anderson, D.M., 2003. A mechanism for offshore initiation of harmful algal blooms in the coastal gulf of Maine. J. Plankton Res. 25, 1131–1138.
McManus, M.A., et al., 2003. Changes in characteristics, distribution and persistence of thin layers over a 48-hour period. Mar. Ecol. Prog. Ser. 261, 1–19.
Melle, W., et al., 2014. The North Atlantic Ocean as habitat for *Calanus finmarchicus*: environmental factors and life history traits. Prog. Oceanogr. 129, 244–284. https://doi.org/10.1016/j.pocean.2014.04.026.
Moe, H., Gjevik, B., Ommundsen, A., 2003. A high resolution tidal model for the coast of Møre and Trøndelag, Mid-Norway. Norweg. J. Geogr. 57, 65–82.
Mork, K.A., Skagseth, O., 2010. A quantitative description of the Norwegian Atlantic current by combining altimetry and hydrography. Ocean Sci. 6, 901–911.
Morrell, L.J., James, R., 2008. Mechanisms for aggregation in animals: rule success depends on ecological variables. Behav. Ecol. 19, 193–201.
Nash, R.D.M., Geffen, A.J., 2004. Seasonal and interannual variation in abundance of *Calanus finmarchicus* (Gunnerus) and *Calanus helgolandicus* (Claus) in inshore waters (west coast of the Isle of Man) in the central Irish Sea. J. Plankton Res. 26, 265–273.
Pineda, J., 1999. Circulation and larval distribution in internal tidal bore warm fronts. Limnol. Oceanogr. 44 (6), 1400–1414.
Planque, B., Graeme, C.H., Ibanez, F., Gamble, J.C., 1997. Large scale spatial variations in the seasonal abundance of *Calanus finmarchicus*. Deep Sea Res. I 44, 315–326.
Pond, S., Pickard, G.L., G. L., 1983. Introductory Dynamical Oceanography. Pergamon Presss, Oxford.
Pringle, J.M., 2007. Turbulence avoidance and the wind driven transport of plankton in the surface Ekman layer. Cont. Shelf Res. 27, 670–678.
Reigstad, M., Wassmann, P., Wexels Riser, C., Øygarden, S., Rey, F., 2002. Variations in hydrography, nutrients and chl-a in the marginal ice-zone and the Central Barents Sea. J. Mar. Syst. 38, 9–29.
Ritz, D.A., 1997. Costs and benefits as a function of group size: experiments on a swarming mysid, *Paramesopodopsis rufa* Fenton. In: Parrish, J.K., Hamner, W.M. (Eds.), Animal Groups in Three Dimensions. Cambridge University Press, Cambridge, pp. 194–206.
Ruiz Etcheverry, L.A., Saraceno, M., Piola, A.R., Strub, P.T., 2016. Sea level anomaly on the Patagonian continental shelf: trends, annual patterns and geostrophic flows. J. Geophys. Res. Oceans 121, 2733–2754. https://doi.org/10.1002/2015JC011265.
Sætre, R., 1999. Features of the central Norwegian shelf circulation. Cont. Shelf Res. 19, 1809–1831.
Sætre, R., 2007. The Norwegian Coastal Current-Oceanography and Climate. Tapir Academic Press, Institute of Marine Research.
Sars, G.O., 1903. An Account of the Crustacea of Norway. Vol IV. Copepoda, Calanoida, 4. BergenMuseum.
Schroeder, I.D., Sydeman, W.J., Sarkar, N., Thompson, S.A., Bograd, S.J., Schwing, F.B., 2009. Winter pre-conditioning of seabird phenology in the California current. Mar. Ecol. Prog. Ser. 303, 211–223.
Shanks, A.L., Shearman, R.K., 2009. Paradigm lost? Cross-shelf distributions of intertidal invertebrate larvae are unaffected by upwelling or downwelling. Mar. Ecol. Prog. Ser. 385, 189–204.
Shanks, A.L., Largier, J.L., Brink, L., Brubaker, J., Hoof, R., 2000. Demonstration of the onshore transport of larval invertebrates by the shoreward movement of an upwelling front. Limnol. Oceanogr. 7, 771–784, 45(1): 230-236.
Shanks, A.L., Brinks, L., L., 2005. Upwelling, downwelling, and cross-shelf transport of bivalve larvae: test of a hypothesis. Mar. Ecol. Prog. Ser. 302, 1–12.
Skagseth, Ø., Drinkwater, K.F., Terrile, E., 2011. Wind- and buoyancy-induced transport of the Norwegian coastal current in the Barents Sea. J. Geophys. Res. 116, C08007. https://doi.org/10.1029/2011JC006996.
Skarðhamar, J., Skagseth, Ø., Albretsen, J., 2015. Diurnal tides on the Barents Sea continental slope. Deep-Sea Res. 97, 40–51.
Sun, B., Liu, C., Wang, F., 2019. Global meridional eddy heat transport inferred from Argo and altimetry observations. Sci. Rep. 9, 1345. https://doi.org/10.1038/s41598-018-38069-2.
Thomson, R.E., Fine, I.V., 2003. Estimating mixed layer depth from oceanic profile data. J. Atmos. Ocean. Technol. 20 (2), 319–329.
Ueda, H., Kuwahara, A., Tanaka, M., Azeta, M., 1983. Underwater observations on copepod swarms in temperate and subtropical water. Mar. Ecol. Prog. Ser. 11, 165–171.
van Rensburg, B.J., Chown, S.L., Gaston, K.J., 2002. Species richness, environmental correlates, and spatial scale: a test using south African birds. Am. Nat. 159, 566–577.

Vargas, C.A., Narvaez, D.A., Piñones, A., Navarrete, S.A., Lagos, N.A., 2006. River plume dynamic influences transport of barnacle larvae in the inner shelf of Central Chile. J. Mar. Biol. Assoc. U. K. 86, 1057–1075.

Vormoor, K., Lawrence, D., Schilchting, L., Wilson, D., Wong, W.K., 2016. Evidence for changes in the magnitude and frequency of observed rainfall vs. snowmelt driven floods in Norway. J. Hydrol. 538, 36–48.

Wallace, M.I., Cottier, F.R., Berge, J., Tarling, G.A., Griffiths, C., Brierley, A.S., 2010. Comparison of zooplankton vertical migration in an ice-free and a seasonally ice-covered Arctic fjord: an insight into the influence of sea ice cover on zooplankton behavior. Limnol. Oceanogr. 55, 831–845. https://doi.org/10.4319/lo.2010.55.2.0831.

Weidberg, N., Basedow, S., 2019. Long-term variability in overwintering copepod populations in the Lofoten Basin: the role of the North Atlantic oscillation and trophic effects. Limnol. Oceanogr. 64, 2044–2058.

Weidberg, N., Lobón, C., López, E., García-Flórez, L., Fernández-Rueda, M.P., Largier, J. L., Acuña, J.L., 2014. Effect of nearshore slicks on meroplankton distributions: role of larval behaviour. Mar. Ecol. Prog. Ser. 506, 15–30. https://doi.org/10.3354/meps10777.

Weidberg, N., DiBacco, C., Pezzola, C., Rebiffe, E., Basedow, S., 2021. Swimming performance of subarctic *Calanus* spp. facing downward currents. Mar. Ecol. Prog. Ser. 665, 47–61.

Wijesekera, H.W., Gregg, M.C., 1996. Surface layer response to weak winds, westerly bursts and rain squalls in the western Pacific warm Pool. J. Geophys. Res. 101, 977–997.

Wishner, K.F., Schoenherr, J.R., Beardsley, R., Chen, C., 1995. Abundance, distribution and population structure of the copepod *Calanus finmarchicus* in a springtime right whale feeding area in the southwestern gulf of Maine. Cont. Shelf Res. 15 (415), 475–507.

Wood., 2006. Generalized Additive Models: An Introduction with R. Chapman and Hall.

Zhou, M., Dorland, R.D., 2004. Aggregation and vertical migration behavior of *Euphausia superba*. Deep-Sea Res. II 51, 2119–2137.

Zhou, M., Zhu, Y., Tande, K.S., 2005. Circulation and behavior of euphausiids in two Norwegian sub-Arctic fjords. Mar. Ecol. Prog. Ser. 300, 159–178.